RSC Advances

ROYAL SOCIETY OF CHEMISTRY

www.rsc.org/advances

Efficient photo-degradation of dyes using $CuWO_4$ nanoparticles with electron sacrificial agents: A combination of experimental and theoretical exploration

Xinjian Xie [a*], Mengyin Liu[b*], Changhong Wang[b], Lei Chen[b], Jianping Xu[c], Yahui Cheng[b], Hong Dong[b], Feng Lu[b], Wei-Hua Wang[b], Hui Liu[b], Weichao Wang[b†]

[a] *School of Material Science and Engineering, Hebei University of Technology, Tianjin 300130, China*

[b] *Department of Electronics and Key Laboratory of Photo-Electronic Thin Film Devices and Technology of Tianjin, Nankai University, Tianjin 300071, China*

[c] *Institute of Material Physics, Key Laboratory of Display Materials and Photoelectric Devices, Ministry of Education, Tianjin University of Technology, Tianjin 300384, China*

**These authors contribute equally*

† Corresponding Author. Tel.: +86 22 23509930; fax: +86 22 23509930.

E-mail address: weichaowang@nankai.edu.cn (W. Wang)

Abstract

$CuWO_4$ is one of the promising photocatalytic materials, responding in the visible light range, to enhance the utilization of solar energy. Here, the $CuWO_4$ nanoparticles have been synthesized via polyol-mediated synthesis method and subsequently characterized by X-ray Diffraction (XRD), scanning electron microscope (SEM), transmission electron microscope (TEM), UV-Vis Spectrophotometer combined with theoretical density functional theory (DFT) calculations. For as-prepared $CuWO_4$ samples, a strong adsorption capacity of organic pollutant MB rather than photodegradation has been observed. The first-principle calculation with Heyd–Scuseria–Ernzerhof (HSE) screened coulomb hybrid functional results indicate that localization of hybridization of O 2*p*-orbitals and Cu 3*d*-orbtials, large electron effective mass and more positive conduction band edge of $CuWO_4$ lead to low carrier mobility and thus the high recombination of excited carriers. Meanwhile, the optical absorption spectrum of experimental observation is consistent with theoretical calculation of pristine $CuWO_4$, demonstrating few defects inhibiting light absorption. To avoid the high rate of recombination of the excited carriers, electron sacrificial agents (H_2O_2, $Na_2S_2O_8$) are utilized to suppress the recombination. The photocatalytic activity is thus largely improved.

Key words

$CuWO_4$, Visible light photocatalysis, Electron sacrificial agent, First-principles calculations

Introduction:

With the increasing problem of environmental pollution, it is important to develop effective technology to clean waste water. Various techniques including biodegradation,[1] ultrafiltration,[2] ion exchange[3] and etc.[4,5,6] have been utilized to achieve this objective. Among these technologies, the advanced oxidation processes (AOP)[7] stand out as a promising way to clean water. The AOP differ from conventional physical and biological water treatment processes as the AOP generate the strong oxidant hydroxyl radicals (•OH) to degrade toxic and refractory pollutants (organic carbon) into simple and harmless inorganic molecules (carbon dioxide and water) without producing secondary pollutants. The •OH generation can be initiated by primary oxidants (H_2O_2 or O_3),[8] energy sources (UV-light, ultrasonic)[9,10] or catalysts.[11] Semiconductor materials could absorb solar energy and excite carries to generate oxidant for further photocatalytic degradation of organic pollutants. For a superior photocatalyst, the band edges should align up with water redox levels. Specifically, the top of valence band (E_V) is required more positive than the redox potential •OH/H_2O (~2.5 V vs. NHE).[12] When solar light is incident on a semiconductor material, the photo-generated electrons and holes react with water and form oxidants (O_2^-, H_2O_2 and O_3) and essentially produce •OH.[13,14]

The semiconductor materials have been used to generate oxidants for several years[15,16] since the photocatalytic splitting of water was discovered on the TiO_2 electrodes by Fujishima and Honda in 1972.[17] To date, anatase TiO_2 dominates the photocatalysis market owing to its low cost, non-toxicity, highly catalytic activity and chemical stability.[18,19] Whereas, TiO_2 with a band gap of 3.2 eV displays a low efficiency (~5%) of utilizing solar energy. In order to ultimately harvest solar energy, it is important to continue searching for visible light driven photocatalysts.[20,21]

$CuWO_4$, as a ternary narrow band gap semiconductor (E_g~2.2 eV), is an ideal high-efficiency semiconductor photocatalyst due to its absorption of visible-light[22,23]

with reasonable valence band alignments with •OH/H_2O energy level. Moreover, the catalytic performances could also be influenced by other factors such as crystallinity, defects and interface, which introduce various electronic structures including band tails,[24] defect states,[25] and interfaces states.[26] These states significantly impact on carrier mobility,[27] carrier's recombination,[28] electronic conductivity[29] and etc,[30] resulting in the variations of the catalytic activity. Without full understanding of the microscopic electronic structures, it would be difficult to further improve the photocatalytic performance. Here, we combined theoretical calculations and experimental methods to link the electronic structures and the catalytic performance of $CuWO_4$. Based on the DFT calculations, the catalytic activity has been improved with the presence of electron capture agents. In such a way, these findings provide insights into further promising photocatalyst design.

In this work, $CuWO_4$ was prepared by polyol-mediated synthesis method. The synthesized samples are characterized by the X-ray Diffraction (XRD), scanning electron microscope (SEM), transmission electron microscopy (TEM) and UV-Vis Spectrophotometer. As-prepared powder displays a strong adsorption capacity of organic pollutant MB rather than photodegradation. First-principle calculations point out that the disadvantage of localized band edge states of hybridization of O 2*p*-orbitals and Cu 3*d*-orbtials causes the high recombination of excited carrier. On the other hand, the experimental optical absorption spectrum of sample is consistent with theoretical calculation of pristine $CuWO_4$ which indicates no problem for our synthesized samples to absorb light. In the presence of electronic sacrificial agent, the excited holes are survived and thus $CuWO_4$ displayed a high photocatalytic performance to degrade the MB dye.

Experiment and Calculation Method

1. Polyol Mediated Synthesis Method

Copper nitrate ($Cu(NO_3)_2 \cdot 3H_2O$, AR, purity ≥ 99.5%) and sodium tungstate ($Na_2WO_4 \cdot 2H_2O$, AR, purity ≥ 99.5%) were used to prepared $CuWO_4$. Copper nitrate (1 mmol) was dissolved in 50 mL diethylene glycol (DEG) and stirred by magnetic stirring at room temperature. Sodium tungstate (1 mmol) was dissolved in 1 mL deionized water and was injected into copper nitrate solution quickly with magnetic stirring. After stirring 3 minutes (min), the products were separated from these suspensions via high-speed centrifuge at 10000 rpm for 5 min and washed by sequential centrifugation/redispersion from/in ethanol for 5 times to remove redundant impurity and DEG completely, and then dried in the oven at 70 °C for 12 hours. In the annealed process, temperature was kept at 500 °C for 1 hour in the air.

2. Evaluation of Photocatalytic Activity

The photocatalytic ability of $CuWO_4$ was evaluated by degradation of MB. The 40 mg $CuWO_4$ powder was dispersed in methylene blue solution (100 ml, 10 mg/L) in a beaker. Subsequently, it was stirred about 30 min in dark in order to reach adsorption-desorption equilibrium. A xenon lamp without filter has been used as the light source and the light intensity remains at 20 $mW \cdot cm^{-2}$ measured by an irradiance meter (Model: FZ-A, Beijing Normal University, China) to reduce solution evaporation. During photogradation of MB solution, the magnetic stirring was kept running. The photodegradation was quantified by monitoring the concentration of MB at its maximum of absorption (664 nm). Commercially available Degussa P25 (nanoscale TiO_2 powder; 80% anatase, 20% rutile; particle diameter: 25 ~ 30 nm) as a reference was used to compare with the photocatalytic performance of $CuWO_4$.

3. Theoretical Model and Calculation Details

The crystal structure of $CuWO_4$ is presented in Fig. 1, containing two formula units with characteristic corner-linked CuO_6 and WO_6 octahedral. The Jahn-Teller effect of the Cu^{2+} cation causes a pseudo-tetragonal elongation of the CuO_6 octahedral. The ab initio calculations were performed based on the density functional theory

(DFT), as implemented in plane-wave based code Vienna ab initio Simulation Package (VASP). The generalized gradient approximation with the Perdew-Burke-Ernzerhof version of the exchange-correlation potential was employed.[31] A large energy cutoff of 550 eV was adopted. Brillouin zone was sampled by the set of (5×4×5) *k*-points for $CuWO_4$ to balance calculation efficiency and accuracy. The convergence criterion for energy is chosen as 10^{-4} eV and the maximum Hellmann-Feynman force acting on each atom is less than 0.01 eV/Å in ionic relaxation calculations. The calculated lattice constants are a = 4.78 Å, b = 6.00 Å, c = 4.93 Å; α = 92.77°, β = 93.51° γ = 81.48°. Considering that GGA usually overestimates the lattice constant slightly,[32,33] the calculated results are in good agreement with the previous results using the GGA functional (a = 4.84 Å, b = 6.05 Å, c = 4.94 Å)[34] and the experimental values (a = 4.69 Å, b = 5.83 Å, c = 4.88 Å).[35] For electronic structure calculations, it is well known that DFT underestimates the band gap, thus the electronic structure with the PBE relaxed structure was calculated using the Heyd–Scuseria–Ernzerhof (HSE)[36] hybrid functional, in which a portion (16%) of Hartree–Fock exchange was mixed with the PBE functional to produce a band gap of ~2.2 eV which is highly consistent with experimental observations.[37]

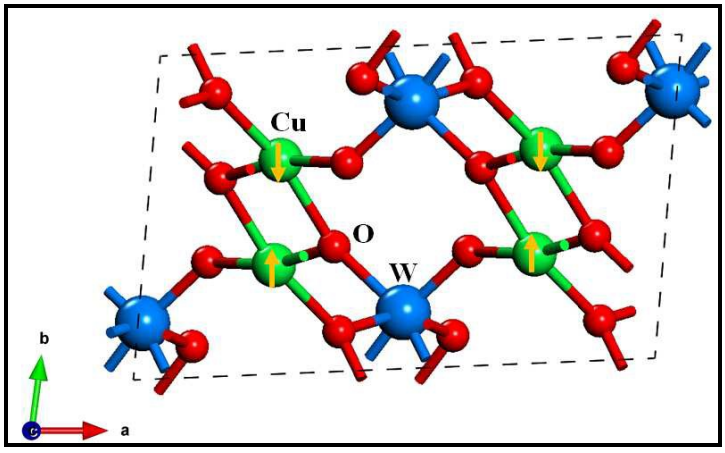

Fig. 1 (color online) The crystal structure of $CuWO_4$, the green, blue and red balls represent Cu, W and O atoms, respectively. Arrows represent the spin directions of Cu.

Results and Discussion

Due to the high polarity of multidentate alcohols such as ethylene glycol, diethylene glycol or glycerol, polyol-mediated synthesis is considered as an effective way to control nucleation and growth of nanoparticles, stabilize the particle surface and avoid agglomeration.[38,39] In this work, we adopted this method to synthesize $CuWO_4$.

The as-prepared $CuWO_4$ powder shows green color (inset in Fig. 2) and the according XRD peaks (Fig. 2) are broadened which indicates the amorphous phase of the sample power. After heating the sample under 500 °C for 2 hours, the color turned into dark grey (inset in Fig. 2) and the XRD pattern displays the formation of the pure phase of $CuWO_4$ (Fig. 2). The color change before and after sample annealing results from the typical quantum size effect.

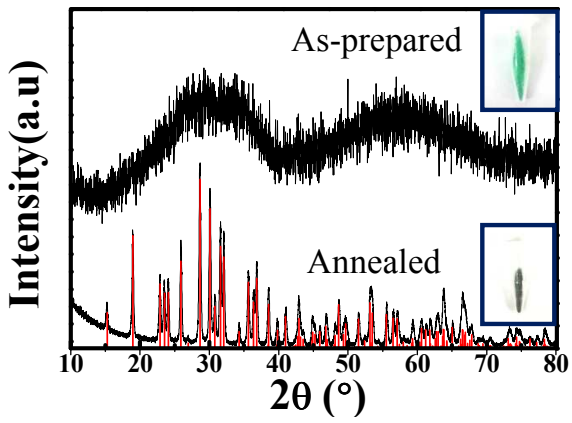

Fig. 2 (color online) XRD pattern of as-prepared and annealed samples.

Fig. 3(a), (b) and (c) describe morphologies of as-prepared sample. Irregular nanoparticles have been observed by SEM (Fig. 3(a)), the grain size varying from 10~20 nm has been verified by TEM (Fig. 3(b), (c)) and the specific surface area is expected to be large. The selected area electron diffraction (SAED) (Fig. 3(c)) shows the blurry spots corresponding to low degree of crystallinity of as-prepared $CuWO_4$.

For the annealed sample, SEM and TEM (Fig. 3(d), (e), (f)) show that the particle size significantly grows up to ~50 nm and nanoparticles seriously reunite due to regrowth and recrystallization during the annealed process. On the other hand, clear spots of SAED (Fig. 3(f)) also identify the improvement of crystallinity after the sample was annealed.

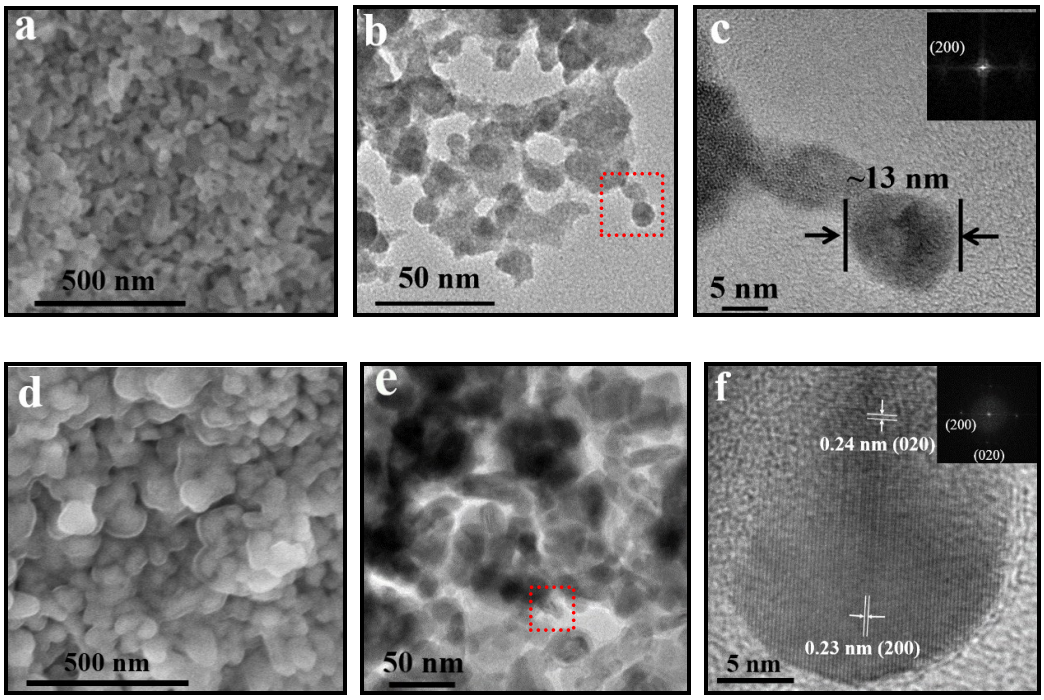

Fig. 3 (color online) SEM, TEM images of as-prepared sample (a), (b) and annealed sample (d), (e); (c) and (f) are magnified high-resolution TEM images of red boxes in (b) and (e), respectively.

For the photodegradation of MB, the as-prepared powder displays a strong adsorption capacity of organic pollutant MB within the first 10 min (Fig. 4(a)). No photodegradation phenomenon has been observed during this period. When continuing increasing observing time larger than 10 min, no more adsorption is displayed since as-prepared $CuWO_4$ has reached its adsorption equilibrium. For the annealed sample, the particle size significantly grows up to ~50 nm and nanoparticles reunite seriously which have been observed by SEM and TEM (Fig. 3d, 3e, 3f). Consequently, the decrease of the surface areas leads to the decrease of MB

adsorption, as shown in Fig. 4(b). Also, the annealed sample displays no photocatalytic behavior. Little variation of the photocatalytic behaviors for the as-prepared sample and the annealed one proves that particle size is not the key to impact the catalytic activity for this case.

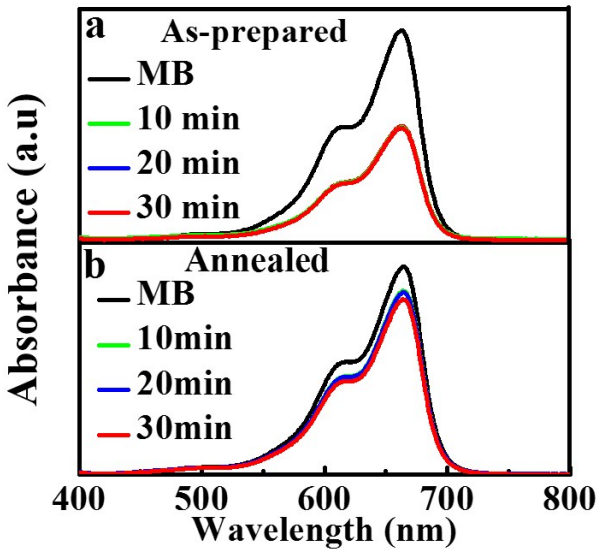

Fig. 4 (color online) The adsorption of MB (a) as-prepared $CuWO_4$ sample and (b) annealed sample.

Intrinsically, two critical factors would govern the photocatalytic activity, i.e. carrier conductivity and optical absorption. For the former one, it is governed by the band edge shapes of $CuWO_4$. The later one is influenced by light absorption spectrum. In order to access the failure mechanism of the photocatalytic performance of $CuWO_4$, electronic structure and optical spectrum should be calculated.

With the advantage of the start-of-art supercomputer and computational algorithm, it is now feasible to access the fundamental electronic structures at the atomic level. In this work, we employed density functional theory (DFT) to explore the electronic structure and optical spectrum of the $CuWO_4$.

Fig. 5 illustrates the calculated band structure along high symmetric k-point B (0.5, 0, 0) - Γ (0, 0, 0) - F (0, 0.5, 0) - Q (0, 0.5, 0.5) - G (0, 0, 0.5) in the first

Brillouin zone. The conduction band minimum (CBM) and valence band maximum (VBM) are located at Γ k-point and Q k-point, respectively, indicating an indirect band gap. The gap value is ~2.2 eV which is highly consistent with experimental result.[37] Also, in the bottom region of conduction band at Γ point, the band is rather flat. By extracting the curvature of the CBM and VBM, we obtained a large the effective mass of electron and hole (m_e^* = 59 m_0, m_h^* = 57 m_0, m_o is free electron mass), resulting in the poor electron and hole conductivity, respectivley.[23]

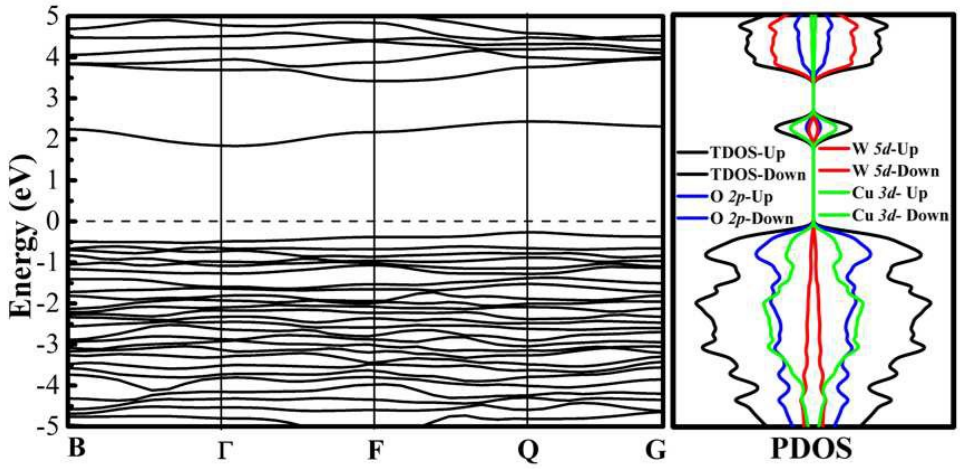

Fig. 5 (color online) The band structure diagram (left panel) and the spin-dependent density of states (right panel) for $CuWO_4$. Fermi level is set at zero eV in both panels.

Fig. 5 also shows the normalized total and projected density of states (PDOS). The spin-up states are identical to the spin-down ones. Thus, $CuWO_4$ presents an anti-ferromagnetic (AFM) ground state with the magnetic moment of 0.68 μ_B for Cu atoms and 0.05 μ_B for O atoms, being consistent with experiment observations of μ_{Cu} = 0.67 μ_B, μ_O = 0.06 μ_B[35] and PBE+U calculation of μ_{Cu} = 0.74 μ_B, μ_O = 0.07 μ_B.[40]

In Fig. 5, the O-2*p* and Cu-3*d* orbitals hybrid and dominate the band edges. More specifically, valance band maximum is mainly composed of the orbital hybridization of oxygen 2*p*-orbitals and copper 3*d*-orbtials, leading to the more positive position of the VBM,[41] and the strong oxidizing property of the excited holes. Therefore, we

speculate that O and Cu could be the activity sites for photocatalysis. The excited hole either directly reacts with organic pollutant molecular to decompose it or reacts with OH^- to produce strong oxidant hydroxyl radicals. Hybridization of Cu-3*d* and O-2*p* results in more positive CBM and narrow band gap which improves the visible-light absorption. Nevertheless, Hybridization of Cu-3*d* and O-2*p* also lead to more positive conduction band edge of $CuWO_4$ compared to H^+/H_2 reduction level in solution.[42] In other words, there is no excited electron acceptor in this photocatalytic system, as a result, excited electrons will gather on the $CuWO_4$ surface and cause more severe surface recombination. Moreover, the localized states of hybridization of O *2p* and Cu *3d* orbitals could lead to the lower carrier mobility, high recombination rate of excited carrier and essentially result in low efficient photocatalytic behavior.

In addition to the material intrinsic electronic properties, optical adsorption is another important factor to govern the photocatalytic activity. For the absorption spectrum of bulk material, it is formatted as:

$$I(\omega) = \sqrt{2}\omega\left[\sqrt{\varepsilon_1^{\,2}(\omega) + \varepsilon_2^{\,2}(\omega)} - \varepsilon_1(\omega)\right]^{1/2}$$

ε_2 and ε_1 are imaginary part and real part of dielectric function, respectively, ω is angular frequency. In order to obtain the absorption spectrum, dielectric constant was calculated via DFT. Fig. 6 (a) and (b) show the calculated results of the imaginary part and real part of dielectric function for $CuWO_4$ along three Cartesian directions, respectively. The optical anisotropy is due to low crystal symmetry and the peculiarities in the crystal structure, i.e., the existence of the bridge-oxygen ions connecting with neighboring CuO_6 and WO_6 complexes. Based on the calculated dielectric function curves, we obtained the theoretical absorption spectrum, as shown in Fig. 6 (c). The light absorption begins about 2.0 eV, corresponding to the electron excitation from the VBM to the CBM (Fig. 6 (c)). Experimentally, the as-prepared and annealed $CuWO_4$ has been used to test the absorption spectrum by UV-Vis Spectrophotometer. For the as-prepared sample, the localized absorption peak

appeared at 1.5 eV as the subgap absorption,[43] which originates from bonding defects induced located states in the forbidden energy gap.[44] This specific subgap absorption helps to improve the visible-light absorption. Compared the theoretical and pure annealed sample absorption spectrum, it is found that they are consistent with each other.[45] This means the light absorption of sample is close to the theoretical value attributed to few defects and impurities hindrance light absorption.[46,47] In other words, our sample shows bulk-like absorption behavior without impacting by defect levels.

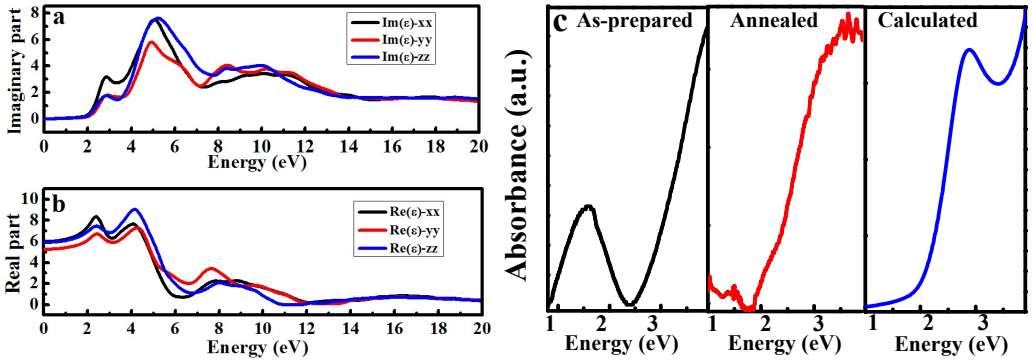

Fig. 6 (color online) The dielectric function of $CuWO_4$ calculated by DFT with HSE functional: (a) imaginary part, (b) real part; (c) The absorption spectrum of $CuWO_4$ obtained from as-prepared sample, annealed sample and theoretical simulation.

On the basis of the theoretical analysis, charge carrier separation would be the key to influence the photocatalytic activity. Thus, promoted separation of the excited carriers would be an effective method to achieve the photocatalytic degradation of MB. In this work, we utilized electron sacrificial agents to examine the charge separation effect on the photocatalytic performance.[48] To confirm the electron capture agent's boost effect on enhancing the photodegradation by as-prepared $CuWO_4$, 1 mmol H_2O_2 or $Na_2S_2O_8$ was dispersed into the MB solution to check the catalytic activity. Fig. 7 (a) indicates that individual H_2O_2 or $Na_2S_2O_8$ displays a limited degraded performance. Surprisingly, in as-prepared $CuWO_4$ (40 mg) combined with 1 mmol H_2O_2 or $Na_2S_2O_8$, we found that MB decomposes rapidly and the MB concentrations reaches to zero within 60 min. (see Fig. 7 (a)). As a

comparison, the as-prepared $CuWO_4$ with electronic capture agents (H_2O_2 or $Na_2S_2O_8$) shows superiority over the same amount of P25 and P25 together with H_2O_2 rather than $Na_2S_2O_8$ in weight in terms of the decomposition of MB. In any case, P25 with $Na_2S_2O_8$ shows the highest efficiency because of the stronger oxidation of $Na_2S_2O_8$ in regards to H_2O_2 (Fig.7 (a)). To examine the role of hole to decompose MB, we utilized $(NH_4)_2C_2O_4$ to exhaust the supply of excited holes, and we found that MB degradation with $(NH_4)_2C_2O_4$ is identical with the self-degradations under UV-Vis light. In other words, hole is the key to decompose MB in our case.

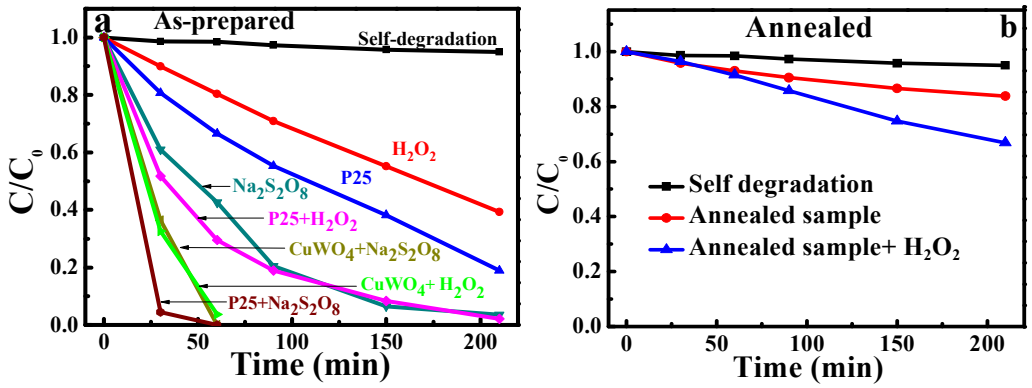

Fig. 7 (color online) The photodegradation of MB (a) as-prepared $CuWO_4$ sample, P25 and (b) annealed sample added electron sacrificial agents, and only electron sacrificial agent without any catalyst.

In order to access the role of electron sacrificial agent to assist in the catalytic performance of the as-prepared $CuWO_4$, we proposed the following schematic diagram to address how electron sacrificial agents improve the photocatalytic efficiency (Fig. 8(a)).

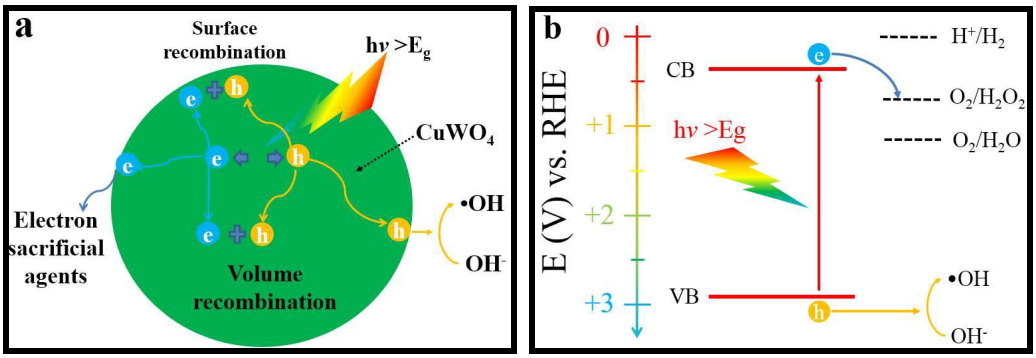

Fig. 8 (color online) (a) Photocatalytic process in the presence of electron sacrificial agents. (b) $CuWO_4$ band alignments with H^+/H_2, O_2/H_2O_2, O_2/H_2O and •OH energy levels.

When the $CuWO_4$ absorbs the photon energy larger than its band gap, the excited electrons (e^-) jump from the valence band to the conduction band and form electron-hole pairs. Parts of them recombine in the as-prepared $CuWO_4$ particles and the others move to the surfaces (Fig. 8 (a)). Meanwhile, owing to the improper band alignment with water redox potentials, as presented in Fig. 8 (b), severe surface recombination occurs as discussed above. Consequently, no enough h^+ combines with OH^- and forms •OH because reactive time (about 10^{-3} s) is much longer than the surface recombining time (about 10^{-12} s). When the electron sacrificial agent (H_2O_2 or $Na_2S_2O_8$) is introduced into MB solution, the excited electrons on surface are captured by electron sacrificial agents. The carrier recombination is thus suppressed and the excited holes have enough time to oxidize the H_2O molecules and generate the strong oxidant •OH. In addition to the role of charge separation from electron sacrificial agents, the strong MB adsorption on the as-prepared $CuWO_4$ surface could be another factor to enhance the photodegradation

For any photocatalyst, crystallinity, electronic structure and possibly surface charge would be crucial to determine the catalytic performance. In the annealed $CuWO_4$ sample with diameter of ~50 nm, even in the presence of electron sacrificial agent, very limited catalytic activity was observed in Fig. 7(b). The limited activity could be attributed to the lower adsorption capacity arising from the high crystallinity

(Fig. 4 (b)). Compared to as-prepared sample, the localized absorption peak at 1.5 eV disappeared in the absorption spectrum of annealed sample (Fig. 6 (c)), decreasing the visible-light absorption and photocatalytic efficiency. From the perspective of surface charge, as an n-type semiconductor,[49] band will upper bend when contacting with solution.[50] As a result, the exited holes tend to transfer to the nanoparticles surface, then directly react with MB or produce •OH which leads to the decomposition of MB pollutants. For the as-prepared amorphous phase, it provide more active sites for surface photogenerated carriers and prevent them from rapid recombination due to high disorders, thus promoting carrier transfer and photocatalytic reactions.[51] After annealing the sample, the particle size increases and thus the active sites significantly reduce. Consequently, the carrier recombination became severe, and the photocatalytic efficiency decreased.

Conclusions

In summary, we have investigated the catalytic activity of $CuWO_4$ nanoparticles in experiment, combined with the DFT electronic structures calculations. The first principle calculation results illustrate that more positive conduction band edge position than H^+/H_2O level, low carrier mobility and high recombination rate of $CuWO_4$ result in an effective adsorption rather than photodegradation of MB for the as-prepared sample. The annealed samples with larger particle size display even a smaller adsorption capability of MB. In the presence of electron sacrificial agents, the photocatalytic efficiency of the as-prepared $CuWO_4$ is significantly improved, due to the suppression of the combination of photo-generation carrier and the enhancement of the formation of •OH. On the other hand, the annealed sample displays rather low catalytic behavior owing to the low adsorption capability.

Acknowledgements

This work is supported by National Natural Science Foundation of China

(11304161, 11104148, 51171082, 21573117 and 11404172), 1000-youth talent program in China, Tianjin Natural Science Foundation (13JCYBJC41100,14JCZDJC37700), the National Basic Research Program of China (973 Program with No. 2014CB931703), Fundamental Research Funds for the Central Universities. We thank the technology support from the Texas Advanced Computing Center (TACC) at the University of Texas at Austin (http://www.tacc.utexas.edu) for providing grid resources that have contributed to the research results reported within this paper.

References

[1] T. Godjevargova, D. Ivanova, Z. Alexieva and N. Dimova, *Process. Biochem.*, 2003, **38**, 915.

[2] N. S. Azmi and K. F. M. Yunos, *Agriculture and Agricultural Science Procedia*, 2014, **2**, 257.

[3] M. F. Rahman, S. Peldszus and W. B. Anderson, *Water Res.*, 2014, **50**, 318.

[4] C. Dorado, C. A. Mullen and A. A. Boateng, *ACS. Sustain. Chem. Eng.*, 2014, **2**, 301.

[5] P. C. Kearney, M. T. Muldoon, C. J. Somich, J. M. Ruth and D. J. Voaden, *J. Agric. Food. Chem.*, 1988, **36**, 1301.

[6] G. Han, S. G. Shin, J. K. Lim, M. Jo and S. Hwang, *AIP. Conf. Proc.*, 2010, **1251**, 209.

[7] R. Andreozzia, V. Caprioa, A. Insolab and R. Marottac, *Catal. Today*, 1999, **53**, 51.

[8] B. T. Oh, Y. S. Seo, D. Sudhakar, J. H. Choe, S. M.Lee, Y. J. Park and M. Cho, *J. Hazard. Mater.*, 2014, **279**, 105.

[9] O. S. Keen, I. Ferrer, E. M. Thurman and K. G. Linden, *Chemosphere*, 2014, **117**, 316.

[10] K. Makino, M. M. Mossoba and P. Riesz, *J. Phys. Chem.*, 1983, **87**, 1369.

[11] H. Czili and A. Horváth, *Appl. Catal. B: Environ.*, 2008, **81**, 295.

[12] S. Pasternak and Y. Paz, *Chem. Phys. Chem.*, 2013, **14**, 2059.

[13] R. Marschall and L. Z.Wang, *Catal. Today*, 2014, **225**, 111.

[14] P. K. J. Robertson, J. M. C. Robertson and D. W. Bahnemann, *J. Hazard. Mater.*,

2012, **211**, 161.

[15] A. Mills and S. L. Hunte, *J. Photoch. Photobio. A*, 1997, **108**, 1.

[16] K. Nakata, T. Ochiai, T. Murakami and A. Fujishima, *Electrochim. Acta.*, 2012, **84**, 103.

[17] A. Fujishima and K. Honda, *Nature*, 1972, **238**, 37.

[18] K. Nakata and A. Fujishima, *J. Photoch. Photobio. C*, 2012, **13**, 169.

[19] J. C. Yu, J. G. Yu, L. Z. Zhang and W. K Ho, *J. Photochem. Photobio. A*, 2002, **148**, 263.

[20] H. L. Wang, T. Deutsch and J. A. Turner, *ECS Trans.*, 2008, **6**, 37.

[21] J. R. Bolton, S. J. Strickler and J. S. Connolly, *Nature*, 1985, **316**, 495.

[22] R. L. Perales, J. R. Fuertes, D. Errandonea, D. M. Garcia and A. Segura, *EPL.*, 2008, **83**, 37002.

[23] K. J. Pyper, J. E. Yourey and B. M. Bartlett, *J. Phys. Chem. C*, 2013, **117**, 24726.

[24] Y. Y. Kang, Y. Q. Yang, L. C. Yin, X. D. Kang, G. Liu and H. M. Cheng, *Adv. Mater.*, 2015, **27**, 4572.

[25] C. X. Yang, T. Y. Li, Z. J. Cheng, H. X. Gan and J. Y. Chen, *Phys. B*, 2012,**407**, 844.

[26] W. C. Wang, S. Y. Chen, P. X. Yang, C. G. Duan and L. W. Wang, *J. Mater. Chem. A,* 2013, **1**, 1078.

[27] J. T. Heath, J. D. Cohen, W. N. Shafarman, D. X. Liao and A. A. Rockett, *Appl. Phys. Lett.*, 2002, **80**, 4540.

[28] A. Layek, B. Manna and A. Chowdhury, *Chem. Phys. Lett.*, 2012, **539**, 133.

[29] J. D. W. Camacho and K. J. Stevenson, *J. Phys. Chem. C*, 2009, **113**, 19082.

[30] T. Scheidt, E. G. Rohwer, H. M. V. Bergmann and H. Stafast, *Phys. Rev. B*, 2004, **69**, 165314.

[31] J. Perdew, K. Burke and M. Ernzerhof, *Phys. Rev. Lett.*, 1996, **77**, 3865.

[32] L. Kihlborg and E. Gebert, *Acta. Cryst.*, 1970, **B26**, 1020.

[33] A. Kuzmin, A. Kalinko and R. A. Evarestov, *Acta Materialia*, 2013, **61**, 371.

[34] J. R. Fuertes, D. Errandonea, R. L. Perales, A. Segura, J. González, F. Rodríguez, F. J. Manjón, S. Ray, P. R. Hernández, A. Muñoz, Z. Zhu and C. Y. Tu, *Phys. Rev. B*, 2010, **81**, 224115.

[35] J. B. Forsyth, C. Wilkinson and A. I. Zvyagin, *J. Phys-Condens. Mat.*, 1991, **3**, 8433.

[36] J. Heyd, G. E. Scuseria and M. Ernzerhof, *J. Chem. Phys.*, 2003, **118**, 8207.

[37] N. Gaillard, Y. C. Chang, A. D. Angelis, S. Higgins and A. A. Braun, *Int. J. Hydrogen. Energy*, 2013, **38**, 3166.

[38] C. Feldmann, *Adv. Funct. Mater.*, 2003, **13**, 101.

[39] P. Schmitt, N. Brem, S. Schunk and C. Feldmann, *Adv. Funct. Mater.*, 2011, **21**, 3037.

[40] M. V. Lalic, Z. S. Popovic and F. R. Vukajlovic, *Comput. Mater. Sci.*, 2011, **50**, 1179.

[41] A. Kudo and Y. Miseki, *Chem. Soc. Rev*., 2009, **38**, 253.

[42] J. E. Yourey and B. M Bartlett, *J. Mater. Chem.*, 2011, **21**, 7651.

[43] M. L. Benkhedir, *Defect Levels in the Amorphous Selenium Bandgap*, Ph.D Thesis, KU Leuven, 2006, 18.

[44] P. W. Anderson, *Phys. Rev.*, 1958, **109**, 1492.

[45] J. E. Yourey, J. B. Kurtz and B. M. Bartlett, *J. Phys. Chem. C,* 2012, **116**, 3200.

[46] F. D. Weerdt and A. T. Collins, *Diam. Relat. Mater.*, 2008, **17**, 171.

[47] E. Burstein, G. Picus, B. Henvis and R. Wallis, *J. Phys. Chem. Solids*,1956, **1**, 65.

[48] J. S. Romao, M. S. Hamdy, G. Mul and J. Baltrusaitis, *J. Hazard. Mater.*, 2015, **282**, 208.

[49] T. Mathew, N. M. Batra and S. K. Arora, *J. Mater. Sci.*, 1992, **27**, 4003.

[50] M. G. Walter, E. L. Warren, J. R. McKone, S. W. Boettcher, Q. X. Mi, E. A. Santori and N. S. Lewis, *Chem. Rev.*, 2010, **110**, 6446.

[51] X. B. Chen, L. Liu, P. Y. Yu and S. S. Mao, *Science*, 2011, **331**, 746.

Table of Contents

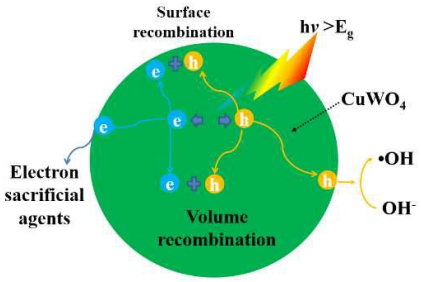

Photocatalytic process of $CuWO_4$ in the presence of electron sacrificial agents.